Supporting Information

3D Printing Microporous Scaffolds from Modular Bioinks Containing Sacrificial, Cell-Encapsulating Microgels

*Alexis J. Seymour, David Kilian, Renato S. Navarro, Sarah M. Hull, and Sarah C. Heilshorn**

List of Supporting Information

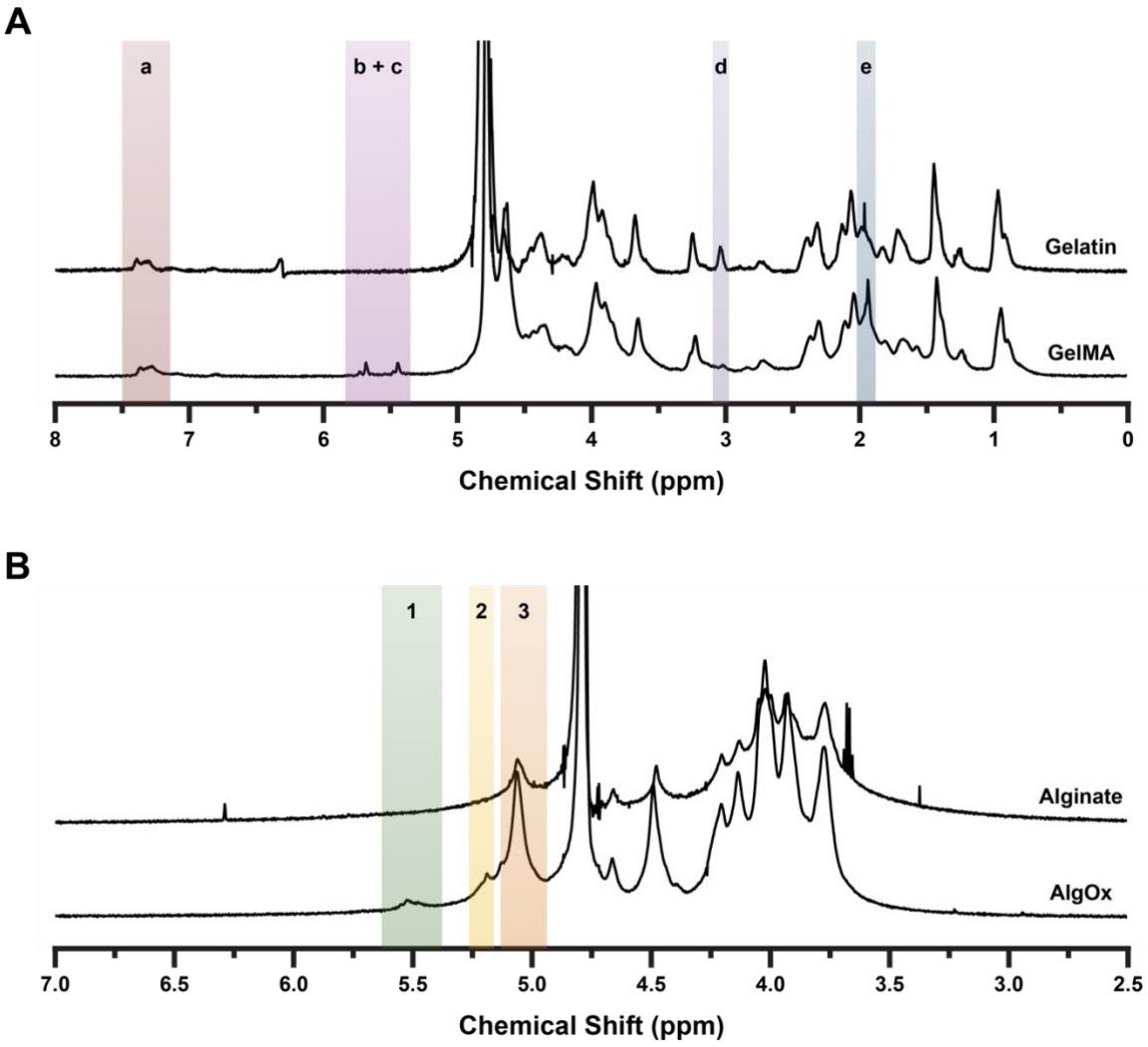

Supporting Figure S1. ^{1}H NMR spectra of biopolymers used for microgel fabrication. (A) ^{1}H NMR spectra of gelatin and GelMA samples in D_2O. Spectra were normalized to the tyrosine peak (7.25 ppm, peak **a**) prior to quantification. The degree of GelMA substitution was then calculated using the ratio of integrals for the lysine-methylene peaks (3.02 ppm, peak **d**) of gelatin and GelMA. The presence of the acrylic protons of grafted methacrylamide groups and lysine groups (5.5 and 5.7 ppm, peaks **b** and **c**) and increased presence of methyl protons of methacrylamide groups (1.75 ppm, peak **d**) in the GelMA spectrum confirms successful gelatin modification with MAA. **(B)** ^{1}H NMR spectra of unmodified and oxidized alginate samples in D_2O with 3-(trimethylsilyl)propionic-2,2,3,3-d_4 acid, sodium salt (TMS) as an internal standard. The degree of alginate oxidation was calculated using the ratio of integrals for existing methyl protons (peak **3**) to methyl protons formed through alginate oxidation (peaks **1** and **2**).

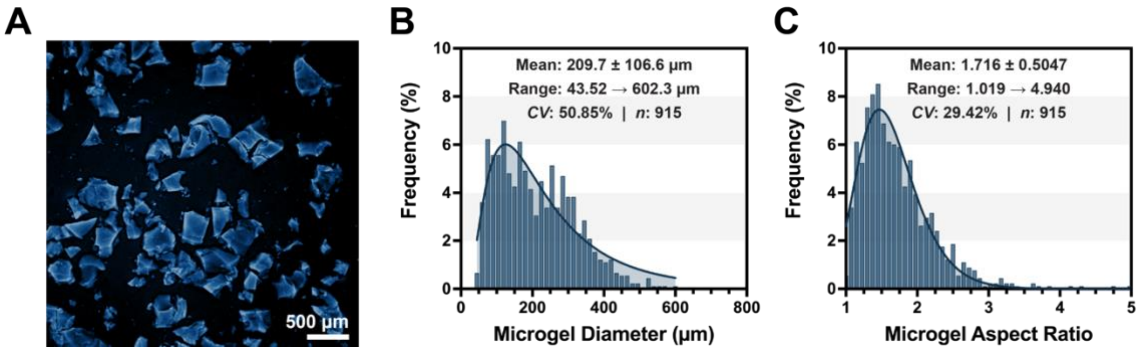

Supporting Figure S2. The diameter and aspect ratio of GelMA microgels produced using extrusion fragmentation. (A) Representative image of GelMA microgels produced using extrusion fragmentation. GelMA microgels were stained with rhodamine B and false-colored blue. Scale bar represents 500 µm. **(B, C)** Quantification of GelMA microgel diameter **(B)** and aspect ratio **(C)** after fragmentation. Data are plotted as a frequency distribution of measured values with a superimposed best-fit curve.

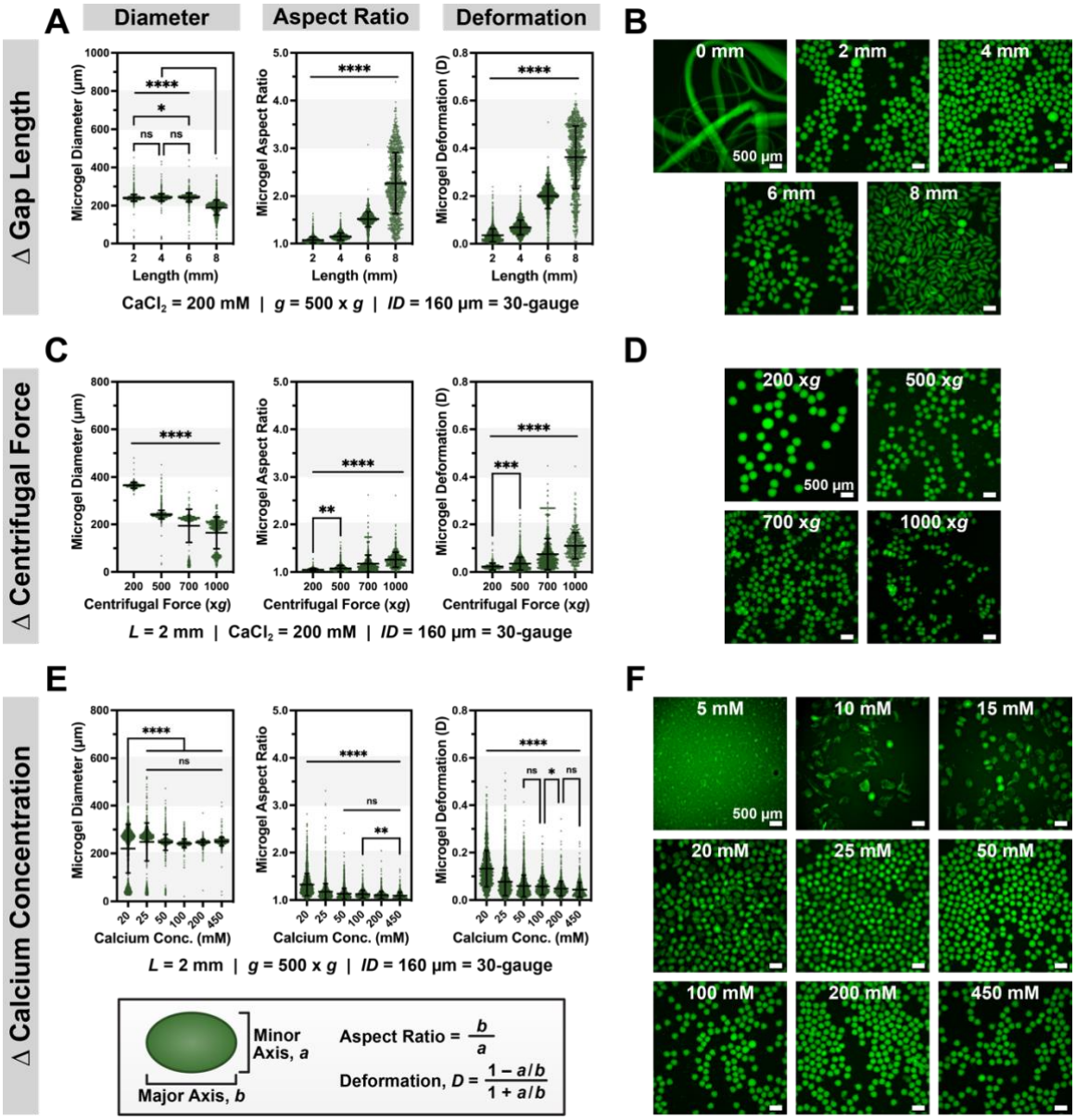

Supporting Figure S3. The effect of fabrication parameters on the morphology of AlgOx microgels produced using the centrifugal microdroplet device. (A, B) The diameter, aspect ratio, and particle deformation **(A)** and representative images **(B)** of AlgOx microgels produced using nozzle-to-reservoir gap lengths (*L*) ranging from 0 to 8 mm. **(C, D)** The diameter, aspect ratio, and deformation **(C)** and representative images **(D)** of AlgOx microgels produced using centrifugal force (x*g*) ranging from 200 to 1000 x *g*. **(E, F)** The diameter, aspect ratio, and deformation **(E)** and representative images **(F)** of AlgOx microgels produced using calcium chloride ($CaCl_2$) concentrations ranging from 5 to 450 mM. Samples fabricated using 5, 10, and 15 mM $CaCl_2$ did not successfully produce microgels and were not quantified. AlgOx microgels contain 2,000-kDa fluorescein isothiocyanate (FITC)-dextran to aid visualization. Scale bars represent 500 μm. Data are plotted as mean ± standard deviation with a superimposed scatter plot of all points. Statistical significance was evaluated using one-way ANOVA with Tukey's post hoc analysis; n.s. = not significant ($p > 0.05$), *$p < 0.05$, **$p < 0.01$, ***$p < 0.001$, ****$p < 0.0001$.

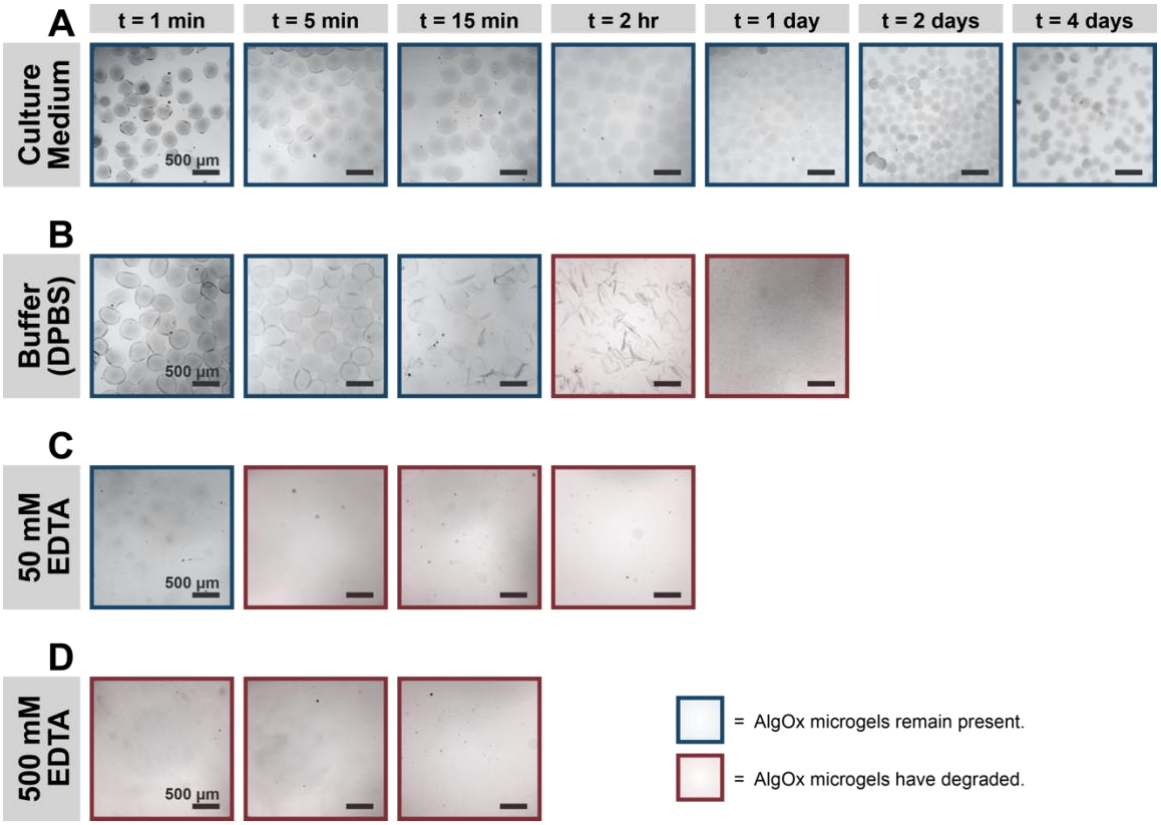

Supporting Figure S4. The degradation of AlgOx microgels incubated at 37 °C in different solutions. (A) Representative images of AlgOx microgels incubated in endothelial cell culture medium demonstrate the persistence of microgels through 4 days. **(B)** Representative images of AlgOx microgels incubated in phosphate-containing buffer (Dulbecco's phosphate-buffered saline, DPBS) demonstrate microgel dissolution after 2 hours. **(C)** Representative images of AlgOx microgels incubated at 37 °C in buffer containing 50 mM ethylenediaminetetraacetic acid (EDTA) demonstrate microgel degradation at 5 minutes. **(D)** Representative images of AlgOx microgels incubated at 37 °C in buffer containing 500 mM EDTA demonstrate immediate microgel degradation. Scale bars in A–D represent 500 µm. Blue outlines indicate samples containing intact AlgOx microgels. Red outlines indicate samples with collapsed or absent AlgOx microgels.

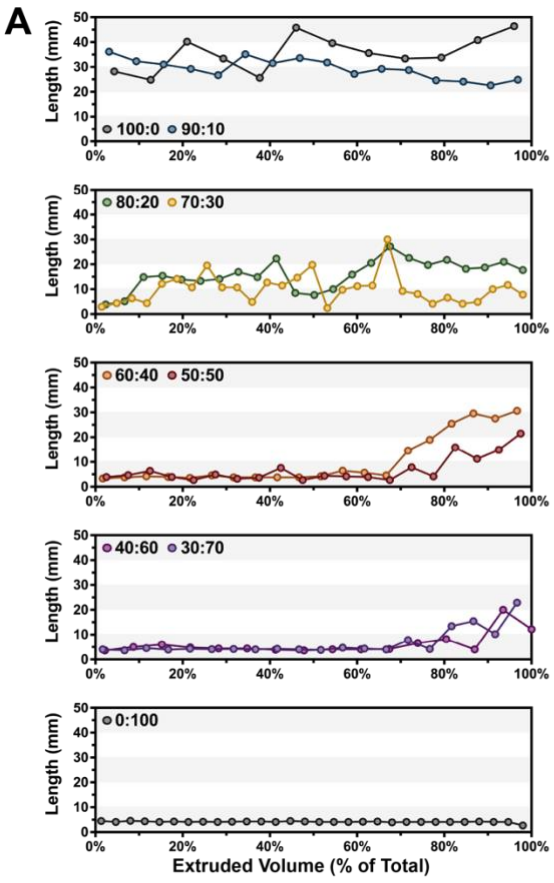

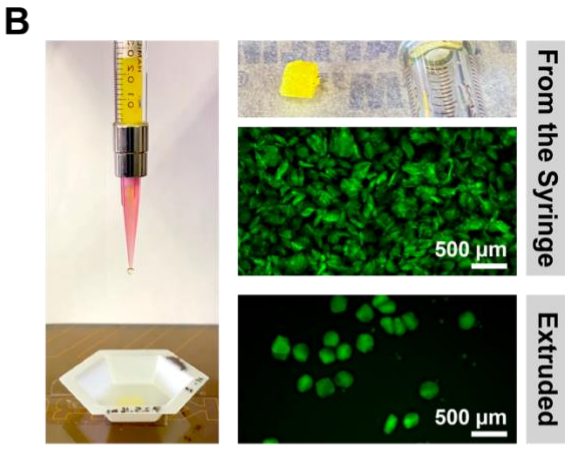

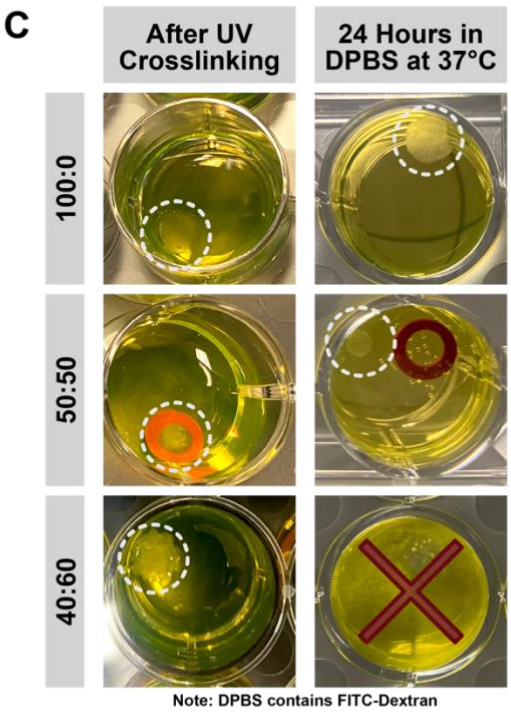

D

Ink	Extrudability	Stability in Culture
100:0	✓	✓
90:10	✓	✓
80:20	✓	✓
70:30	✓	✓
60:40	✓	✓
50:50	✓	✓
40:60	✓	✗
30:70	✓	✗
20:80	✗	✗
10:90	✗	✗
0:100	✗	✗

Supporting Figure S5. The extrudability and post-crosslinking stability of GelMA:AlgOx microgel inks. (A) Representative data of measured filament length throughout extrusion for eight extrudable inks (100:0 through 30:70) and one ink that was not extrudable (0:100). **(B)** Inks that were not extrudable – such as the 0:100, all-AlgOx ink (shown) – extruded the liquid phase as droplets (left) and formed a compressed plug in the syringe (top right). Fluorescence microscopy reveals that AlgOx microgels crush in the syringe (right middle), and few microgels are extruded (right bottom). AlgOx microgels contain 2,000-kDa FITC-dextran to aid visualization. Scale bars represent 500 µm. **(C)** Representative photographs showing cast disks of UV-crosslinked

GelMA:AlgOx microgel blends before (left) and after (right) incubation in phosphate-buffered saline at 37 °C. The ink blends 100:0 through 50:50 remained intact. Inks with greater than 50% AlgOx microgels (i.e., 40:60 through 0:100) dissociated. **(D)** Table summarizing GelMA:AlgOx ink extrudability and stability.

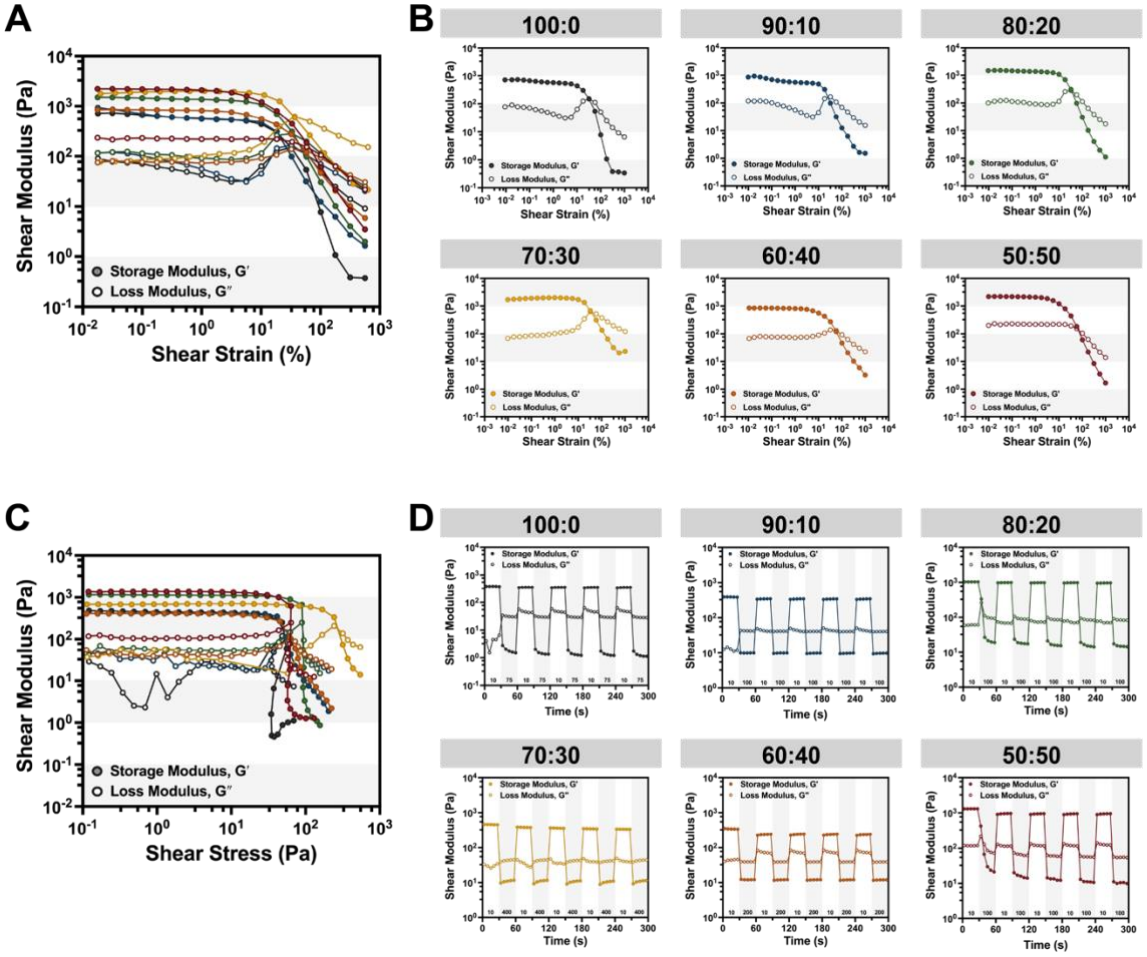

Supporting Figure S6. Additional rheological characterization for all uncrosslinked GelMA:AlgOx inks. (A) Storage moduli (G', filled symbols) and loss moduli (G'', open symbols) of GelMA:AlgOx microgel inks as a function of shear strain (0.01–1000% strain, 1 Hz); same as Figure 3C. **(B)** Individual plots showing the storage moduli (G', filled symbols) and loss moduli (G'', open symbols) of GelMA:AlgOx microgel inks as a function of shear strain (0.01–1000% strain, 1 Hz) for each GelMA:AlgOx microgel ink. **(C)** Storage moduli (G', filled symbols) and loss moduli (G'', open symbols) of GelMA:AlgOx microgel inks as a function of shear stress (0.1–1000 Pa, 1 Hz). The shear stress amplitude sweep was used to determine high and low shear stress values for subsequent cyclic loading tests. **(D)** Cyclic loading tests showing the storage moduli (G', filled symbols) and loss moduli (G'', open symbols) of GelMA:AlgOx inks in response to alternating periods of low (white bar) and high (gray bar) shear stress as listed for each ink.

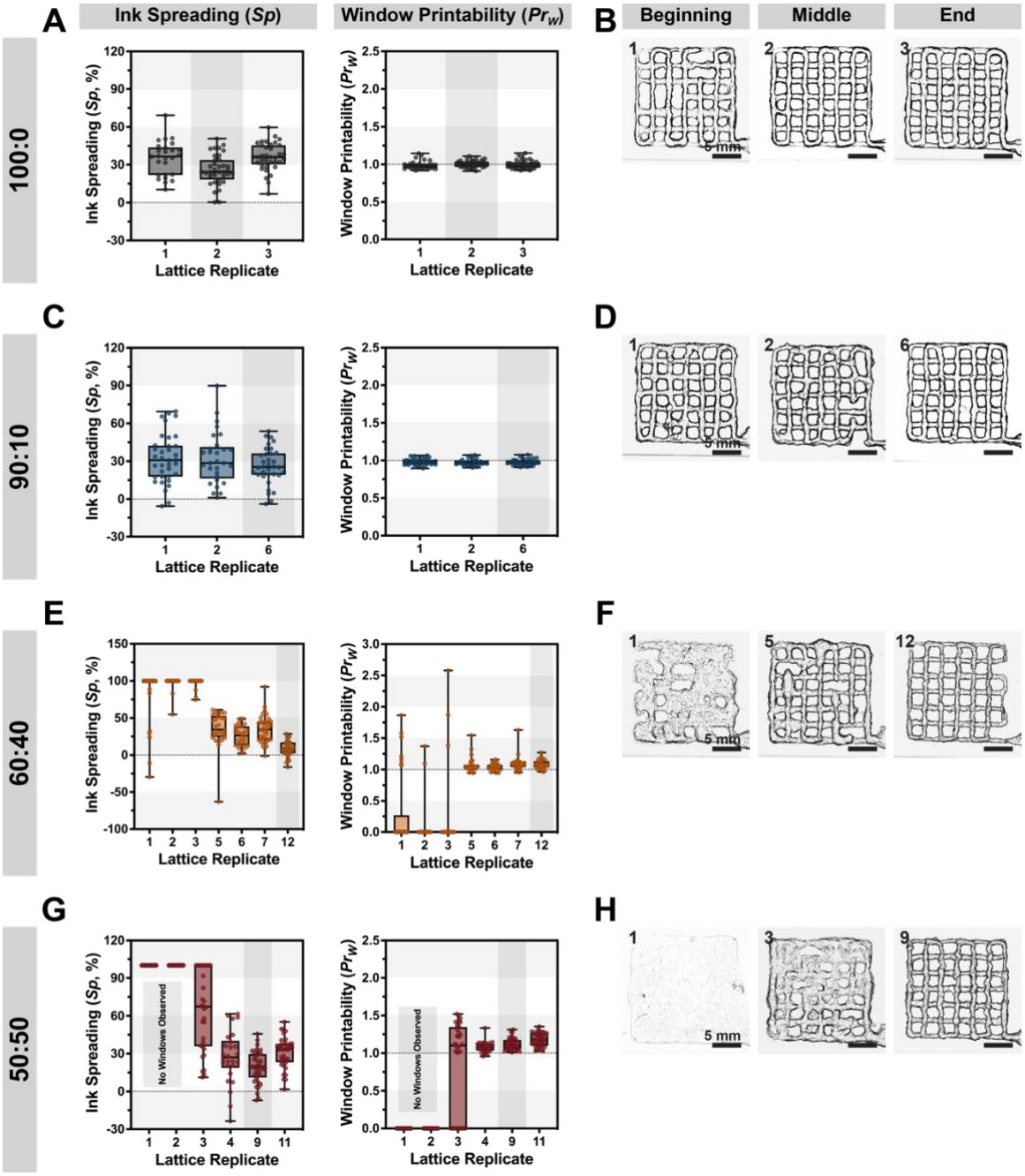

Supporting Figure S7. Consecutive lattice replicates printed with selected GelMA:AlgOx inks. (A, C, E, G) The ink spreading (*Sp*), window printability (Pr_W), and **(B, D, F, H)** corresponding selected brightfield microscopic images of 15 mm by 15 mm lattices printed with the 100:0, 90:10, 60:40, and 50:50 inks. High GelMA microgel content inks, such as 100:0 and 90:10, show consistent lattice shape fidelity throughout extrusion. In contrast, intermediate blends like 60:40 and 50:50 show poor shape fidelity at the outset of extrusion that improves over time. Data are plotted as a box and whisker plot, with whiskers showing the minimum and maximum values and a superimposed scatter plot of all points. Representative lattices shown in Figure 4 are indicated by a gray bar. All scale bars represent 5 mm.

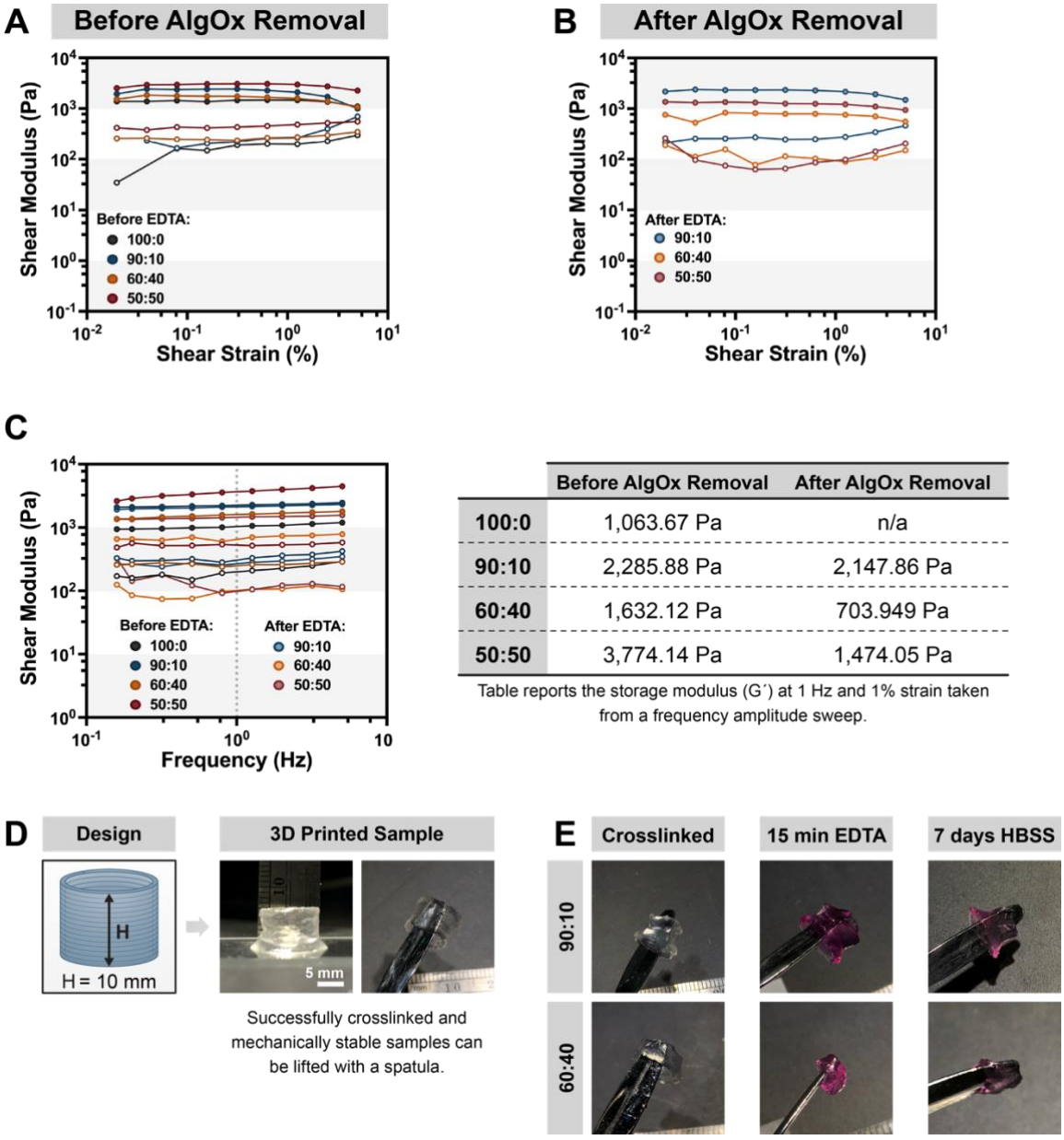

	Before AlgOx Removal	After AlgOx Removal
100:0	1,063.67 Pa	n/a
90:10	2,285.88 Pa	2,147.86 Pa
60:40	1,632.12 Pa	703.949 Pa
50:50	3,774.14 Pa	1,474.05 Pa

Table reports the storage modulus (G´) at 1 Hz and 1% strain taken from a frequency amplitude sweep.

Supporting Figure S8. Investigating the stability of UV-crosslinked GelMA:AlgOx inks before and after AlgOx microgel dissolution. (A) Storage moduli (G', filled symbols) and loss moduli (G'', open symbols) of UV-crosslinked GelMA:AlgOx microgel inks prior to AlgOx microgel degradation as a function of shear strain (0.01–10% strain, 1 Hz). **(B)** Storage moduli (G', filled symbols) and loss moduli (G'', open symbols) of UV-crosslinked GelMA:AlgOx microgel inks after complete AlgOx microgel dissolution as a function of shear strain (0.01–10% strain, 1 Hz). **(C)** Storage moduli (G', filled symbols) and loss moduli (G'', open symbols) of UV-crosslinked GelMA:AlgOx microgel inks before and after AlgOx microgel degradation as a function of oscillation frequency (0.1–10 Hz, 1% strain) beside a table of the storage moduli for each condition at 1 Hz and 1% strain. **(D)** Ink stability was tested by 3D printing a 10 mm tall, thin-walled cylinder ('Design'). After printing and UV-crosslinking, samples were physically inspected to test mechanical integrity. **(E)** Representative images showing cylinders printed from GelMA:AlgOx microgel inks immediately after UV-crosslinking, after incubation in EDTA, and after incubation for 7 days in buffer (Hank's balanced salt solution, HBSS).

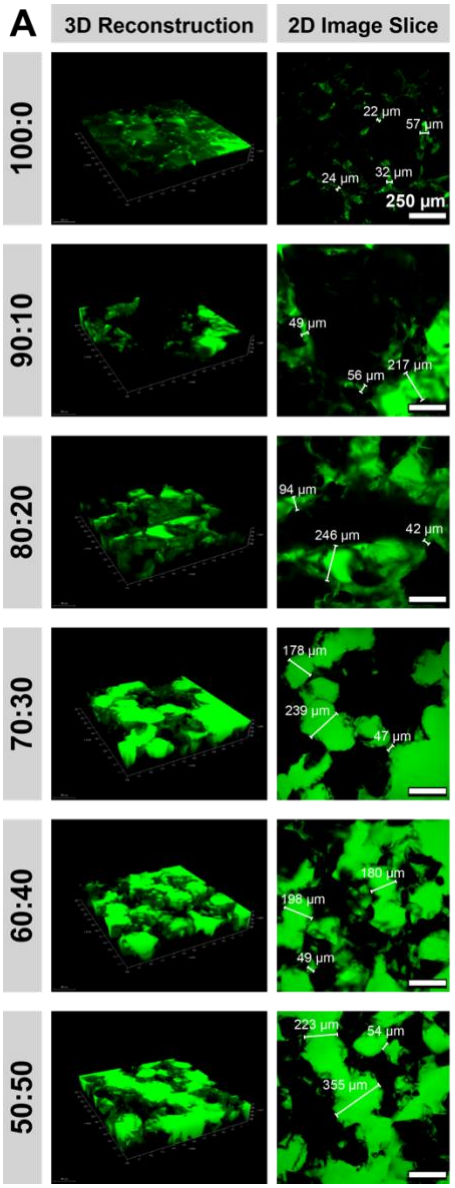

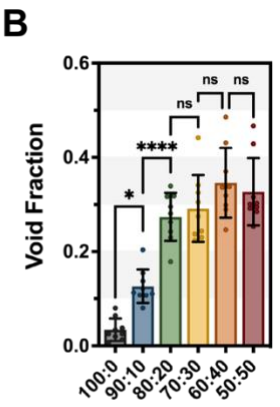

	Void Fraction	*n*
100:0	0.03397 ± 0.02382	9
90:10	0.1263 ± 0.03580	9
80:20	0.2739 ± 0.05096	9
70:30	0.2914 ± 0.07110	9
60:40	0.3462 ± 0.07389	9
50:50	0.3268 ± 0.07151	9

Table reports mean ± std dev.
n = number of images.

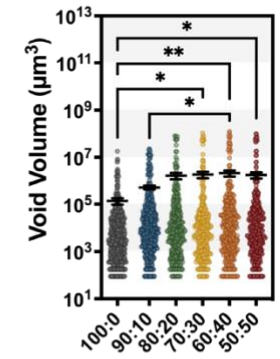

	Void Volume (µm³)	*n*
100:0	138,221 ± 42,838	539
90:10	532,736 ± 105,502	520
80:20	1,664,130 ± 494,219	361
70:30	1,874,170 ± 573,783	341
60:40	2,130,196 ± 608,234	372
50:50	1,781,924 ± 518,393	398

Table reports mean ± std error of mean.
n = number of voids measured.

Supporting Figure S9. Additional characterization of voids within GelMA:AlgOx inks. (A) Representative 3D reconstructions and 2D images of void space within GelMA:AlgOx ink blends. Microgels are shown in black. The void space is filled with 2,000-kDa FITC-dextran and is shown in green. Scale bars represent 250 µm. **(B)** The void fraction of all GelMA:AlgOx microgel inks (same as Figure 5C) beside a table of measured values. Data are displayed as mean ± standard deviation, with a superimposed scatter plot of all points. **(C)** The measured volume of individual voids beside a table of measured values. Data are shown as a scatter plot with lines depicting mean ± standard error. Statistical significance tested by one-way ANOVA with Tukey's post hoc analysis; n.s. = not significant ($p > 0.05$), *$p < 0.05$, **$p < 0.01$, ***$p < 0.001$, ****$p < 0.0001$.

A

		Diameter (μm)	Aspect Ratio	Deformation
Acellular	Mean	246.4	1.132	0.0596
	SD	33.30	0.1147	0.0452
	n		2285	
With Cells	Mean	248.9	1.179	0.0784
	SD	26.33	0.1453	0.0549
	n		1848	

L = 2 mm | *g* = 500 x *g* | $CaCl_2$ = 50 mM | *ID* = 160 μm

B

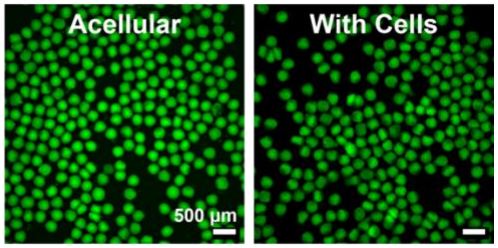

Supporting Figure S10. Comparison of AlgOx microgel diameter, aspect ratio, and deformation made with and without HUVEC. (A) The diameter, aspect ratio, and deformation of AlgOx microgels produced in the absence ('Acellular') and presence ('With Cells') of HUVEC. **(B)** Representative images of AlgOx microgels produced with and without (acellular) HUVEC. Fabrication parameters are listed. AlgOx microgels contain 2,000-kDa FITC-dextran to aid visualization. Scale bars represent 500 μm.

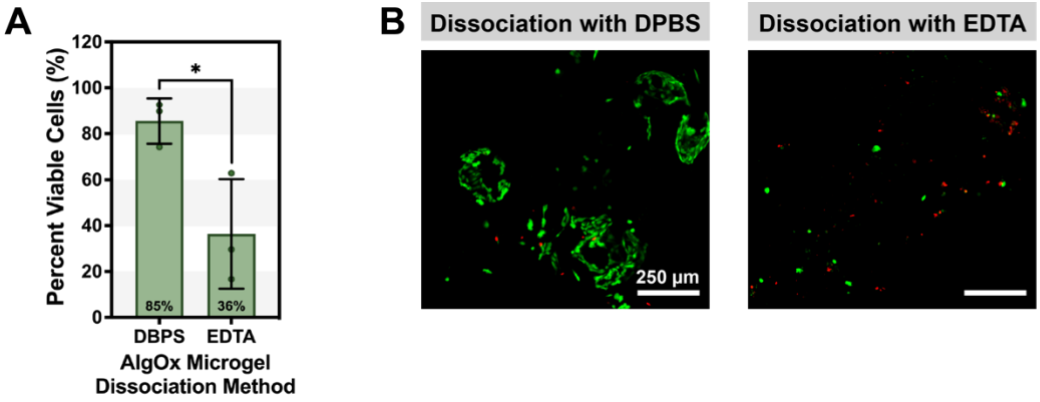

Supporting Figure S11. The viability of endothelial cells within GelMA:AlgOx microgel inks after AlgOx microgel dissolution. (A) The viability of human umbilical vein endothelial cells (HUVEC) cultured within printed GelMA:AlgOx microgel inks after treatment with either Dulbecco's phosphate-buffered saline (DPBS) or ethylenediaminetetraacetic acid (EDTA) to dissociate AlgOx microgels. Data are plotted as mean ± standard deviation, with a superimposed scatter plot of all points. Statistical significance tested by one-way ANOVA with Tukey's post hoc analysis; n.s. = not significant ($p > 0.05$), *$p < 0.05$, **$p < 0.01$, ***$p < 0.001$, ****$p < 0.0001$. **(B)** Representative images of HUVEC within GelMA:AlgOx microgel inks treated with either DPBS or EDTA and stained with Live/Dead™ (green: viable cells; red: membrane-damaged cells). Scale bars represent 250 μm.

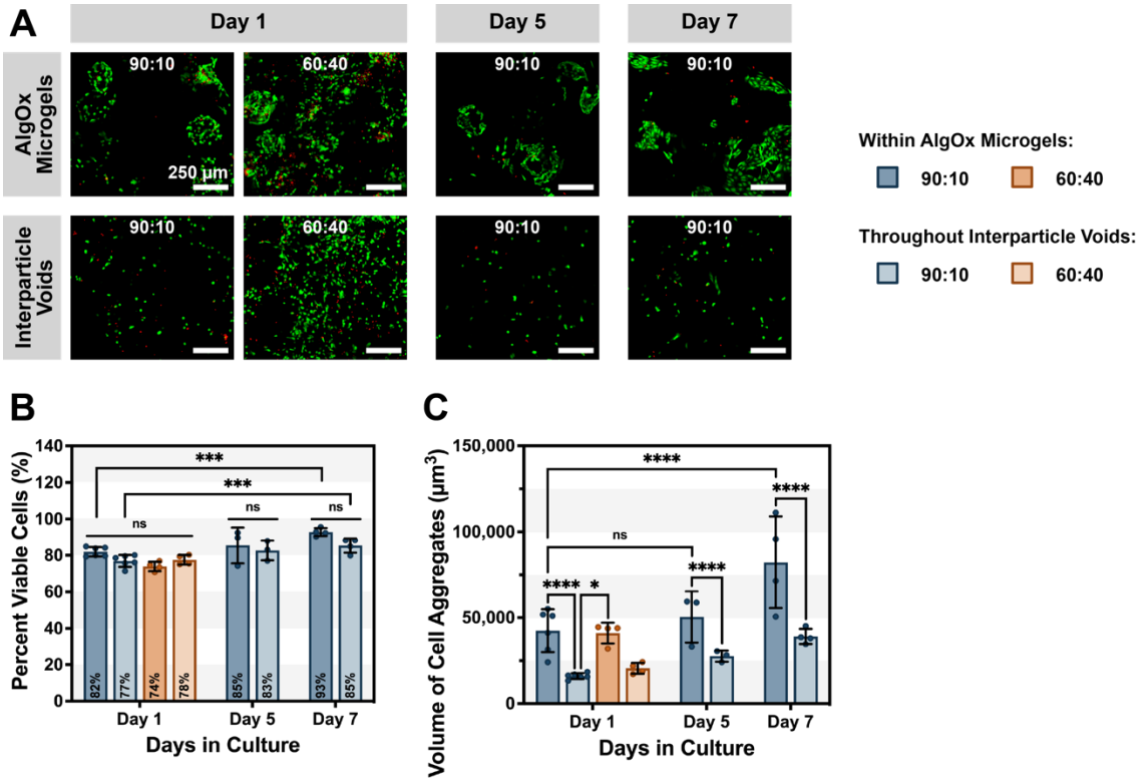

Supporting Figure S12. The effect of cell location on endothelial cells printed within GelMA:AlgOx microgel inks. (A) Representative images of HUVEC cultured within GelMA:AlgOx microgel inks and stained with Live/Dead™ (green: viable cells; red: membrane-damaged cells). Scale bars represent 250 µm. **(B)** The viability of human umbilical vein endothelial cells (HUVEC) cultured within printed GelMA:AlgOx microgel inks after either encapsulation within AlgOx microgels or blending throughout interparticle voids. **(C)** The volume of HUVEC – single cells and aggregates – cultured within printed GelMA:AlgOx microgel inks after either encapsulation within AlgOx microgels or blending throughout interparticle voids. Data in B and C are plotted as mean ± standard deviation, with a superimposed scatter plot of all points. Statistical significance tested by two-way ANOVA with Tukey's post hoc analysis; n.s. = not significant ($p > 0.05$), *$p < 0.05$, **$p < 0.01$, ***$p < 0.001$, ****$p < 0.0001$.

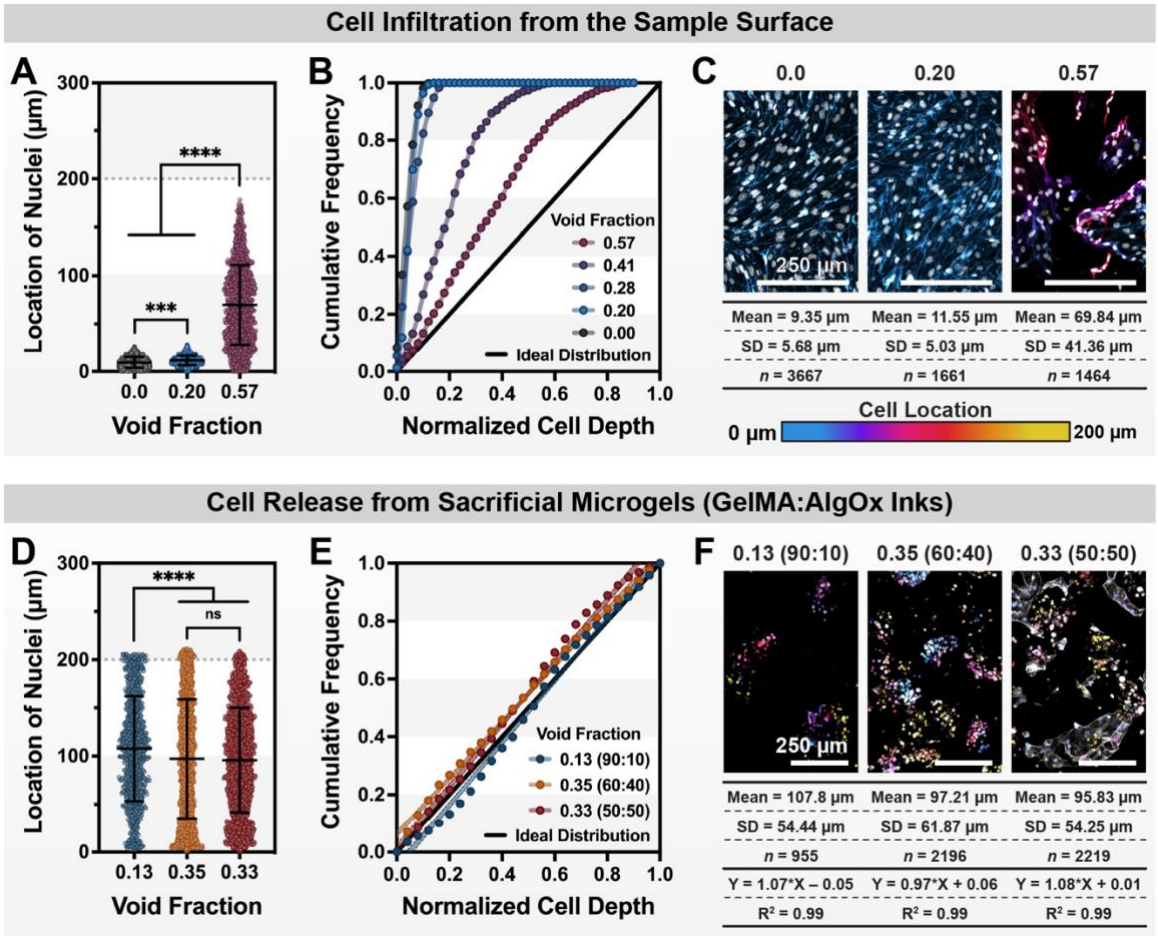

Supporting Figure S13. Comparison of cell distributions within printed constructs resulting from either infiltration from the sample surface or cell release from sacrificial AlgOx microgels. (A, D) The vertical position (along the *z*-axis) of cell nuclei after seven days of infiltration into **(A)** or culture within **(D)** inks with a range of void fractions as quantified from confocal microscopic images. Data are plotted as mean ± standard deviation with a superimposed scatter plot of all points. Statistical significance tested by one-way ANOVA with Tukey's post hoc analysis; n.s. = not significant ($p > 0.05$), *$p < 0.05$, **$p < 0.01$, ***$p < 0.001$, ****$p < 0.0001$. **(B, E)** The nuclear position was normalized by the maximum depth (200 µm) and plotted as a cumulative frequency distribution (circles). Data points in **(B)** are connected; data in **(E)** are fitted to trendlines (colored lines), and the 95% confidence intervals are shown (filled areas between dashed lines). The data are compared to an ideal distribution, where cells are uniformly distributed along the *z*-axis (trendline: $Y = X$). **(C, F)** Representative images of HUVEC that migrated into **(C)** or were cultured within **(F)** 3D printed disks with a range of void fractions. The mean cell position, standard deviation (*SD*), and number of counted nuclei (*n*) are shown for all. Trendlines and *R*-square values are listed in **(F)**. Nuclei in **(C)** are white; nuclei in **(F)** are false-colored to represent the *z*-position within the printed ink (blue: 0 µm; yellow: 200 µm). The actin cytoskeleton in **(C)** is false-colored to represent the *z*-position (blue: 0 µm; yellow: 200 µm); the actin cytoskeleton in **(F)** is false-colored white. Scale bars represent 250 µm. Data in A–C are reanalyzed from our previous work using GelMA:gelatin microgel inks.[18]